Author/s:
Gawthrop, P;Lee, KY;Halaki, M;O'Dwyer, N

Title:
Human stick balancing: An intermittent control explanation

Date:
2013-12-01

Citation:
Gawthrop, P., Lee, K. Y., Halaki, M. & O'Dwyer, N. (2013). Human stick balancing: An intermittent control explanation. Biological Cybernetics, 107 (6), pp.637-652. https://doi.org/10.1007/s00422-013-0564-4.

Persistent Link:
https://hdl.handle.net/11343/282995

Biological Cybernetics manuscript No.
(will be inserted by the editor)

Peter Gawthrop · Kwee-Yum Lee · Mark Halaki · Nicholas O'Dwyer

Human Stick Balancing: An Intermittent Control Explanation

August 3, 2013

Abstract There are two issues in balancing a stick pivoting on a finger tip (or mechanically on a moving cart): maintaining the stick angle near to vertical and maintaining the horizontal position within the bounds of reach or cart track.

The (linearised) dynamics of the angle are second order (although driven by pivot acceleration) and so, as in human standing, control of the angle is not, by itself very difficult. However, once the angle is under control, the position dynamics are, in general, fourth order. This makes control quite difficult for humans (and even an engineering control system requires careful design).

Recently, three of the authors have experimentally demonstrated that humans control the stick angle in a special way: the closed-loop inverted pendulum behaves as a non-inverted pendulum with a virtual pivot somewhere between the stick centre and tip and with increased gravity. Moreover, they suggest that the virtual pivot lies at the radius of gyration (about the mass centre) above the mass centre.

This paper gives a continuous-time control-theoretical interpretation of the virtual-pendulum approach. In particular, by using a novel cascade control structure, it is shown that the horizontal control of the virtual pivot becomes a second order problem which is much easier to solve than the generic fourth-order problem. Hence, the use of the virtual pivot approach allows the control problem to be perceived by the subject as two separate second order problems rather than a single fourth-order problem and the control problem is therefore simplified.

The theoretical predictions are verified using the data previously presented by three of the authors and analysed using a standard parameter estimation method. The experimental data indicates that, although all subjects adopt the virtual pivot approach, the less expert subjects exhibit larger amplitude angular motion and poorly-controlled translational motion.

It is known that human control systems are delayed and intermittent, and therefore the continuous-time strategy cannot be correct. However, the model of intermittent control used in this paper is based on the virtual pivot continuous-time control scheme, handles time-delays and, moreover masquerades as the underlying continuous-time controller. In addition, the event-driven properties of intermittent control can explain experimentally-observed variability.

Peter Gawthrop
Dept. of Electrical and Electronic Engineering, Melbourne School of Engineering, University of Melbourne, VIC 3010, Australia.
E-mail: peter.gawthrop@unimelb.edu.au

Kwee-Yum Lee
School of Exercise Science, Australian Catholic University, Strathfield, NSW 2135, Australia.
E-mail: kwee.lee@acu.edu.au

Mark Halaki
Discipline of Exercise and Sport Science, The University of Sydney, NSW 2006, Australia.
E-mail: mark.halaki@sydney.edu.au

Nicholas O'Dwyer
School of Human Movement Studies, Charles Sturt University, Bathurst, NSW 2795, Australia.
E-mail: nodwyer@csu.edu.au

1 Introduction

As discussed in a recent survey (Boubaker 2012), the inverted pendulum has been a standard control engineering laboratory experiment for many years. Typically, such experiments involve the inverted pendulum being freely pivoted about a point on an actuated moving object (often called the cart); torque is not directly applied to the pendulum, but indirectly via the acceleration of the actuated moving object. The dynamical equations and corresponding control algorithms are presented, for example, by Astrom and Furuta (2000), Fantoni and Lozano (2002) and Gawthrop et al. (2009b).

The inverted pendulum has been used as a model of human standing (Fitzpatrick and McCloskey 1994; Loram and Lakie 2002) and a number of computational theories have been proposed including those of Bottaro et al.

(2005, 2008), Asai et al. (2009), Gawthrop et al. (2011), Kowalczyk et al. (2011) and Suzuki et al. (2012). However, in the case of human standing the torque is applied directly to the inverted pendulum via the muscle/tendon subsystem. Thus the control engineering laboratory experiments referred to in the previous paragraph are not directly relevant.

A more direct analogy to the inverted pendulum control experiment is found in the human balancing of a stick with the base on the finger or the palm of the hand. Experimental results have been obtained, and theoretical explanations have been given, by a number of authors including Cabrera and Milton (2002), Mehta and Schaal (2002), Milton et al. (2008), Milton et al. (2009) and Lee et al. (2012).

A key issue in both human and machine stick balancing is that, in addition to stabilising the angular motion of the stick around a vertical configuration, the horizontal motion of the stick needs to be stabilised. If the horizontal motion is unconstrained in the machine case, the cart will run off the end of the track; in the human case, the reach of the subject will be exceeded. Thus, for example, Gawthrop et al. (2009b) include a control loop to explicitly regulate the horizontal motion in the context of a control laboratory experiment.

The dynamics of the stick balancing system, including both the angular and lateral motion of the stick is fourth order. Although not an issue for control system design in the machine case, it is a problem for humans. Lee et al. (2012) observed that humans oscillate the stick in such a way that "the behaviour of the balanced stick resembled angular simple harmonic motion of a torque-assisted physical pendulum, with a translating suspension point". Based on this observation, this paper suggests that humans approximately split the fourth order system into two, non-interacting second-order systems separately defining the angular and lateral motions of the stick. The structure of the two subsystems is such that they are amenable to cascade control (Goodwin et al. 2001). It is known that humans can successfully simultaneously control two non-interacting second-order systems (Oytam et al. 2005).

The human visuo-motor control system contains time delays (Kleinman et al. 1970, 1971; Gawthrop et al. 2008; Loram et al. 2009; Nijhawan and Wu 2009; Scholl et al. 2009; Stepan 2009; Gawthrop et al. 2009a; Volkinshtein and Meir 2011; Karniel 2011; Milton 2011; Insperger et al. 2013) and is intermittent (Craik 1947; Vince 1948; Navas and Stark 1968; Neilson et al. 1988; Cabrera and Milton 2002; Loram et al. 2012; van de Kamp et al. 2013). For this reason, although a purely continuous-time control system can be used for machine control, such an approach cannot explain human stick balancing. However, the approach to intermittent control proposed by Gawthrop et al. (2011) shows how to convert a continuous-time controller designed for a delay-free system into a predictive intermittent controller. Although, this intermittent controller introduces both delay and intermittency, it can *masquerade* as the underlying continuous time control system. The current paper proposes a novel form of cascade intermittent control to explain the previously observed experimental data presented by Lee et al. (2012).

The paper is organised as follows. Section 2 presents the basic equations of the finger-balanced stick. Section 3 presents the decomposition of the fourth order system into two second order systems and proposes a cascade control structure based on th4e virtual pivot approach. Section 4 gives an intermittent version of the continuous cascade controller of Section 3. Section 5 presents some illustrative simulation results and Section 6 discusses the experimental data. Section 7 shows how parameter estimation methods can be used to extract key parameters from experimental data. Section 8 concludes the paper.

2 Inverted Pendulum Dynamics

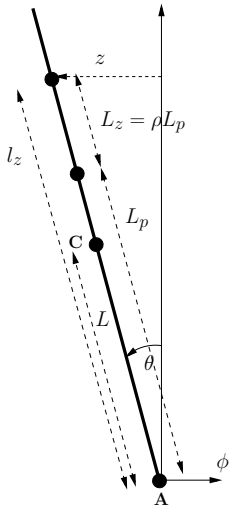

Fig. 1 Balanced Stick at angle θ to the vertical. **A**: Actual pivot with position ϕ and acceleration $u = \ddot{\phi}$. **C** centre of mass. **P** centre of percussion; **V**: virtual pivot location. For small θ, the horizontal position z of the virtual pivot at **V** is given by $z = l_z\theta - \phi$.

With reference to Figure 1, consider an inverted pendulum comprising a stick which freely rotates (with angle θ measured anti-clockwise from the vertical) about a pivot **A** at the lower end, which is in turn constrained to translate horizontally with distance ϕ from some reference. As discussed elsewhere (Astrom and Furuta 2000; Gawthrop et al. 2009b), the linearised (about $\theta = 0$) equations of motion are:

$$J\ddot{\theta} - mgL\theta = mLu \tag{1}$$

$$\text{and } \ddot{\phi} = u \tag{2}$$

where θ is the pendulum angle measured anti-clockwise from the vertical, J is the moment of inertia about the pivot at **A**, m the pendulum mass, L the distance from the pivot to the centre of mass at **C** and g is the gravitational acceleration constant. The control signal u is the horizontal acceleration $\ddot{\phi}$ of the pivot.

It is convenient to define the *equivalent length*[1] L_p given by:

$$L_p = \frac{J}{mL} \tag{3}$$

Equation (1) then simplifies to:

$$L_p\ddot{\theta} - g\theta = u \tag{4}$$

The corresponding point **P** appears in Figure 1.

Using Equations (1) and (2), together with Equation (3), system transfer functions are:

$$G_\theta = \frac{\theta}{u} = \frac{1}{L_p s^2 - g} \tag{5}$$

$$G_\phi = \frac{\phi}{u} = \frac{1}{s^2} \tag{6}$$

The transfer function G_θ has two real poles at $s = \pm a_\theta$ where

$$a_\theta = \sqrt{\frac{g}{L_p}} \tag{7}$$

The pole at $s = a_\theta$ corresponds to unstable, or toppling behaviour; it follows that feedback control is needed to stabilise this system. The transfer function G_ϕ has two poles at $s = 0$; these correspond to drifting velocity and position and therefore feedback control is needed to stabilise this system as well.

With reference to Figure 1, and assuming that the angle θ is small, consider the horizontal motion z of the point **V** a distance l_z above the pivot at **A**.

$$z = l_z\theta - \phi \tag{8}$$

$$= [l_z G_\theta - G_\phi]\, u \tag{9}$$

$$= \left[l_z \frac{1}{L_p s^2 - g} - \frac{1}{s^2}\right] u \tag{10}$$

$$= G_{zu} u \tag{11}$$

$$\text{where } G_{zu} = \frac{L_z s^2 + g}{s^2(L_p s^2 - g)} \tag{12}$$

$$\text{and } L_z = l_z - L_p \tag{13}$$

Using Equations (5) and (12), the transfer function G_z relating z and θ can be written as:

$$\frac{z}{\theta} = G_z(s) = \frac{G_{zu}(s)}{G_\theta(s)} = \frac{L_z s^2 + g}{s^2} \tag{14}$$

[1] The equivalent length L_p is also the distance from the pivot to the centre of percussion

Assuming that $L_z > 0$ (that is $l_z > L_p$), the transfer function relating θ to z has a pair of imaginary zeros at $s = \pm j\omega_z$ where:

$$\omega_z = \sqrt{\frac{g}{L_z}} \tag{15}$$

The significance of these zeros is that if $\theta(t)$ is sinusoidal with frequency ω_z, and the pendulum has been stabilised so that initial conditions die away, the virtual pivot at **V** will be motionless. This point is examined further in the next section.

3 Continuous-time Control

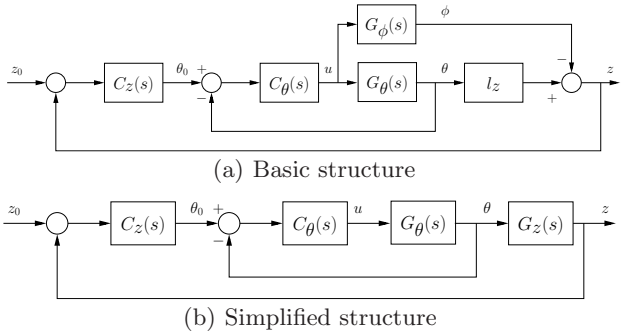

(a) Basic structure

(b) Simplified structure

Fig. 2 Cascade control structure. (a) $G_\theta(s)$ (5) and $G_\phi(s)$ (6) relate the control signal u to the stick angle θ and pivot position ϕ respectively. (b) The simplified structure uses $G_z(s)$ to relate z to θ (14). The transfer function C_θ is then designed to stabilise the stick in such a way that it appears to rotate about the virtual pivot point **V**. The transfer function C_z is then chosen to stabilise the horizontal motion z of the virtual pivot.

The control scheme considered in this paper has the cascade structure of Figure 2. In particular, the inner loop comprises the transfer function $G_\theta(s)$ and the corresponding controller transfer function $C_\theta(s)$. This is designed as discussed by Lee et al. (2012) to make the stick appear to behave as a pendulum with pivot point V (Figure 1); the reference θ_0 would be zero if just the pendulum angle were to be controlled. The design of this inner loop is given in Section 3.1. The outer loop comprises the controller with transfer function $C_z(s)$ which controls the horizontal position z of the virtual pivot to the desired value of z_0 (typically zero) by manipulating the reference θ_0 of the inner loop. As discussed in Section 3.2 this is simplified by the special properties of the inner loop created by the virtual pivot concept of Lee et al. (2012).

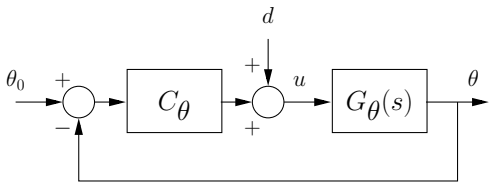

Fig. 3 Frequency-matched control of angle. The stick angle dynamics $G_\theta(s)$ of Equation (5) are controlled using the proportional controller C_θ of Equation (17); d represents motor noise.

3.1 Frequency-matched control of angle

As noted in Section 2, the transfer function relating angle θ to horizontal motion z has a pair of imaginary zeros corresponding to the frequency ω_z of Equation (15). The purpose of this section is to design a controller which gives a closed-loop transfer function causing both u and θ to oscillate at the frequency ω_z. This is done by designing a closed-loop transfer function H_θ with a pair of imaginary poles corresponding to the frequency ω_z.

Consider the feedback system of Figure 3 where the feedback controller[2] is

$$u = C_\theta(\theta_0 - \theta) + d \tag{16}$$

$$\text{where } C_\theta = (k_\theta + 1)g \tag{17}$$

where θ_0 is the reference angle and the disturbance d is introduced by motor noise. The closed-loop system relating θ_0 to θ is:

$$\theta = H_\theta\,(\theta_0 + d_\theta) \tag{18}$$

$$\text{where } H_\theta = \frac{(k_\theta+1)g}{L_p s^2 - g + (k_\theta+1)g} = \frac{(k_\theta+1)g}{L_p s^2 + k_\theta g} \tag{19}$$

$$\text{and } d_\theta = \frac{1}{(k_\theta+1)g} d \tag{20}$$

$$\text{Choosing } k_\theta = \frac{1}{\rho} \tag{21}$$

$$\text{where } \rho = \frac{L_z}{L_p} \tag{22}$$

$$\text{then } H_\theta = \frac{(1+\rho)g}{L_z s^2 + g} \tag{23}$$

$$\text{and } d_\theta = \frac{\rho}{(1+\rho)g} d \tag{24}$$

The denominator of H_θ is identical to the numerator of G_z (14).

Following Lee et al. (2012), one choice of l_z is at the radius of gyration above the centre of mass; thus $l_z = L + r_g$ where r_g is the radius of gyration about the centre of mass. Using Equations (3) and (13), this gives

$$L_z = L + r_g - L_p \tag{25}$$

and the corresponding gain k_θ is given by Equation (21).

The closed-loop system poles are the roots of the denominator of H_θ (23) and are at

$$s = \pm j\omega_\theta \tag{26}$$

$$\text{where } \omega_\theta = \sqrt{\frac{g}{L_z}} \tag{27}$$

Controller design with closed-loop poles on the imaginary axis gives a closed-loop system which is oscillatory and thus on the boundary of stability. In practice, an element of damping must be introduced via velocity (or other phase-advance) feedback. For the purposes of simulation Equation (26) is replaced by:

$$s = (-\xi_\theta \pm j)\omega_\theta \tag{28}$$

where ξ_θ is given in Table 1.

3.2 Control of position.

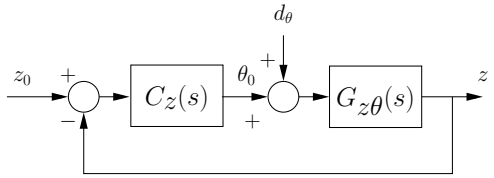

Fig. 4 Control of position. As shown in Equation (30), the transfer function $G_{z\theta}(s)$ represents the closed-loop dynamics of the inner (angle) control of Section 3.1. This can be controlled using the proportional + derivative controller $C_z(s)$ of Equation (32). d_θ represents the effect of d (Figure 3) and is given by Equation (24).

The horizontal position of the pendulum needs to be controlled to prevent the pivot position growing without bound. This task is greatly simplified by the virtual pendulum approach. In particular, the frequency-matched controller cancels the zero associated with the transfer function relating the pivot position ϕ to the virtual pivot position z. With reference to Figure 4 and using Equations (14) and (23), the transfer function $G_{z\theta}$ relating the angle controller reference θ_0 to the horizontal displacement z of the virtual pivot is given by

$$z = G_{z\theta}\,(\theta_0 + d_\theta) \tag{29}$$

$$\text{where } G_{z\theta} = \frac{z}{\theta_0} = G_z H_\theta = \frac{L_z s^2 + g}{s^2}\,\frac{(1+\rho)g}{L_z s^2 + g} = \frac{(1+\rho)g}{s^2} \tag{30}$$

[2] This corresponds to Lee et al. (2012), Equation (13), where $k = k_\theta + 1$ and $d = \theta_0 = 0$.

Note that the term $L_z s^2 + g$ is cancelled from the numerator and denominator. Thus the transfer function $G_{z\theta}$ relating the virtual pivot position z to the angle set-point θ_0 is just a double integrator with gain $(1+\rho)g$; this is much easier to control than a fourth order system. With reference to Figure 4, the proportional + derivative controller:

$$\theta_0 = C_z(s)(z_0 - z) \tag{31}$$

$$\text{where } C_z(s) = \frac{k_v s + k_p}{(1+\rho)g} \tag{32}$$

will give the closed-loop system:

$$z = H_z\,(z_0 + d_z) \tag{33}$$

$$\text{where } H_z = \frac{k_v s + k_p}{s^2 + k_v s + k_p} \tag{34}$$

$$\text{and } d_z = \frac{(1+\rho)g}{k_v s + k_p} d_\theta = \frac{\rho}{k_v s + k_p} d \tag{35}$$

The closed loop system polynomial is completely specified by the control gains k_p and k_v and can be written as:

$$s^2 + k_v s + k_p = s^2 + 2\xi_z \omega_z + \omega_z^2 \tag{36}$$

$$\text{where } \omega_z = \sqrt{k_p} \tag{37}$$

$$\text{and } \xi_z = \frac{k_v}{2\sqrt{k_p}} \tag{38}$$

The closed-loop transfer function has poles at

$$s = (-\xi_z \pm j)\omega_z \tag{39}$$

3.3 State-space formulation

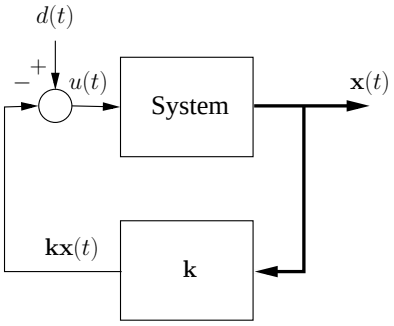

Fig. 5 State-space control formulation. "System" is the state-space system representation of Equation (43) and the state-feedback gain vector $\mathbf{k}$ is given by Equation (57). Vector signals are represented by thick lines.

The development in Section 3.1 and 3.2 is expressed in transfer function terms. This section give an alternative state-space approach which will be used in Section 4 as the basis for intermittent control.

As discussed in Sections 3.1 and 3.2, the use of the virtual pivot point at a distance l_z from the pivot means that, with suitable control of angle θ, the dynamics of the horizontal position z of the virtual pivot become simple. For this reason the system state x is based on θ and z and is defined as

$$\mathbf{x} = \begin{bmatrix} \dot\theta \\ \theta \\ \dot z \\ z \end{bmatrix} \tag{40}$$

Using Equations (2), (4) and (8)

$$\begin{aligned} \ddot z &= l_z \ddot\theta - \ddot\phi \\ &= \frac{l_z g}{L_p}\theta + \left(\frac{l_z}{L_p} - 1\right) u \end{aligned} \tag{41}$$

Using Equations (13) and (22), Equation (41) can be rewritten as:

$$\ddot z = (1+\rho)g\theta + \rho u \tag{42}$$

Using Equation (4) and (42), the open-loop system can be written in state-space form as:

$$\dot{\mathbf{x}} = \mathbf{A}\mathbf{x} + \mathbf{B}u \tag{43}$$

$$\text{where } \mathbf{A} = \begin{bmatrix} 0 & \frac{g}{L_p} & 0 & 0 \\ 1 & 0 & 0 & 0 \\ 0 & (1+\rho)g & 0 & 0 \\ 0 & 0 & 1 & 0 \end{bmatrix} \tag{44}$$

$$\text{and } \mathbf{B} = \begin{bmatrix} \frac{1}{L_p} \\ 0 \\ \rho \\ 0 \end{bmatrix} \tag{45}$$

Turning now to closing the inner (angle) loop, the control signal defined by Equations (16) and (21) is

$$u = \frac{1+\rho}{\rho} g(\theta_0 - \theta) + d \tag{46}$$

$$= \mathbf{k}_\theta(\mathbf{x}_\theta \theta_0 - \mathbf{x}) + d \tag{47}$$

$$\text{where } \mathbf{k}_\theta = \begin{bmatrix} 0 & \frac{1+\rho}{\rho} g & 0 & 0 \end{bmatrix} \tag{48}$$

$$\text{and } \mathbf{x}_\theta = \begin{bmatrix} 0 & 1 & 0 & 0 \end{bmatrix}^T \tag{49}$$

Substituting Equation (46) into (43) and using Equations (44) and (45) gives the partially closed-loop system:

$$\dot{\mathbf{x}} = \mathbf{A}_\theta x + \mathbf{B}_\theta(\theta_0 + d_\theta) \tag{50}$$

$$\text{where } \mathbf{A}_\theta = \mathbf{A} - \mathbf{B}\mathbf{k}_\theta = \begin{bmatrix} 0 & -\frac{g}{L_z} & 0 & 0 \\ 1 & 0 & 0 & 0 \\ 0 & 0 & 0 & 0 \\ 0 & 0 & 1 & 0 \end{bmatrix} \tag{51}$$

$$\text{and } \mathbf{B}_\theta = \mathbf{B}\mathbf{k}_\theta \mathbf{x}_\theta = (1+\rho)g \begin{bmatrix} \frac{1}{L_z} \\ 0 \\ 1 \\ 0 \end{bmatrix} \tag{52}$$

The outer loop control is given by (31). In state-space terms it becomes:

$$\theta_0 = \mathbf{k}_z(\mathbf{x}_z z_0 - \mathbf{x}) \tag{53}$$

$$\text{where } \mathbf{k}_z = \frac{1}{(1+\rho)g}\begin{bmatrix}0 & 0 & k_v & k_p\end{bmatrix} \tag{54}$$

$$\text{and } \mathbf{x}_z = \begin{bmatrix}0 & 0 & 0 & 1\end{bmatrix}^T \tag{55}$$

Finally, when $z_0 = 0$, the overall state feedback controller is given by:

$$\begin{aligned} u &= \mathbf{k}_\theta(\mathbf{x}_\theta\theta_0 - \mathbf{x}) + d \\ &= \mathbf{k}_\theta(-\mathbf{x}_\theta\mathbf{k}_z\mathbf{x} - \mathbf{x}) + d \\ &= -\mathbf{k}\mathbf{x} + d \end{aligned} \tag{56}$$

$$\text{where } \mathbf{k} = \mathbf{k}_\theta(\mathbf{x}_\theta\mathbf{k}_z + \mathbf{I}) \tag{57}$$

and $\mathbf{I}$ is the unit matrix.

The corresponding closed-loop system is then given by:

$$\dot{\mathbf{x}} = \mathbf{A}_c\mathbf{x} + \mathbf{B}d \tag{58}$$

$$\text{where } \mathbf{A}_c = \mathbf{A} - \mathbf{B}\mathbf{k} \tag{59}$$

Alternatively, using standard pole-placement theory (Kwakernaak and Sivan 1972; Goodwin et al. 2001), the 4×1 gain vector $\mathbf{k}$ can be designed to place the four closed-loop poles at the locations defined by Equation (28), that is at:

$$s = (-\xi_\theta + j)\omega_\theta,\ (-\xi_\theta - j)\omega_\theta,\ (-\xi_z + j)\omega_z,\ (-\xi_z - j)\omega_z \tag{60}$$

This continuous time control strategy cannot, by itself, explain human control balancing for two reasons: as discussed in the Introduction, the human visuo-motor control systems contains time delays which are not included in this analysis and human control systems are known to be intermittent. However, this continuous-time control system can serve as the underlying design method of the intermittent controller of Gawthrop et al. (2011). This is discussed in the next section.

4 Intermittent Control

The paper by Gawthrop et al. (2011) provides a computational theory of human control systems based on intermittent control. As discussed by Shadmehr and Wise (2005) and Todorov and Jordan (2002), computational level theories – in the sense of Marr (1982) – try to explain mathematically why a physiological system behaves as it does and provide a computable algorithm to explain the behaviour. In this section, the general equations of intermittent control (Gawthrop et al. 2011) are simplified for the particular case of stick balancing.

Intermittent control – in the sense of Gawthrop et al. (2011) – is based on an underlying continuous-time system and corresponding control design. In the context of this paper, the state-space formulation of Section 3.3, describing the cascade control structure of Section 3, provides this underlying design. In particular, the system with the state space representation of Equations (40) and (43)–(45), together with the feedback controller of Equations (56) and (57), defines the underlying design for this paper. In particular, pole-placement design is used based on the poles appearing in expression (60).

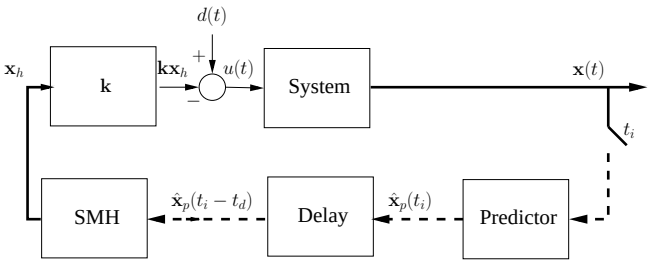

Fig. 6 Intermittent Control. In contrast to the continuous-time control of Figure 5, intermittent control samples the state $\mathbf{x}$ at times t_i and reconstructs the state between samples using a system-matched hold (SMH). The time delay t_d is compensated by a predictor. Dashed lines correspond to sampled signals and firm lines to continuous signals. Vector signals are represented by thick lines.

As described by Gawthrop et al. (2011), Section 3.1, intermittent control makes use of three time frames:

1. **continuous-time**, within which the controlled system evolves, which is denoted by t.
2. **discrete-time** points at which feedback occurs indexed by i. Thus, for example, the discrete-time instants are denoted t_i and the corresponding estimated state is $\hat{\mathbf{x}}_i = \hat{\mathbf{x}}(t_i)$. The ith intermittent interval Δ_i is defined as
$$\Delta_i = t_{i+1} - t_i \tag{61}$$
3. **intermittent-time** is a continuous-time variable, denoted by τ, restarting at each intermittent interval. Thus, within the ith intermittent interval:
$$\tau = t - t_i \tag{62}$$

It is assumed that the human controller is not only intermittent but has a time-delay t_d.

As discussed by Smith (1967), the psychological refractory period (PRP) of Telford (1931) was used by Vince (1948) to explain the human response to double stimuli. In the context of the intermittent control model of this paper, the computational equivalent of the psychological refractory period is to impose a lower bound Δ_{min} on each intermittent interval $\Delta_i > 0$ (61):

$$\Delta_i > \Delta_{min} > 0 \tag{63}$$

The *system-matched hold* (SMH) (Gawthrop et al. 2011), Section 3.2, is a model of the *closed-loop* system with state $\mathbf{x}_h$ which is intermittently reset to the predicted system state $\mathbf{x}_p$. Thus $\mathbf{x}_h$ provides an approximate

replacement for the predicted state $\mathbf{x}_p$ of the closed-loop system in between the intermittent samples of $\mathbf{x}_p$. The equations of the SMH are:

$$\begin{cases} \frac{d}{d\tau}\mathbf{x}_h(\tau) & = \mathbf{A}_c\mathbf{x}_h(\tau) \\ \mathbf{x}_h(0) & = \mathbf{x}_p(t_i - t_d) \end{cases} \tag{64}$$

and $\mathbf{A}_c$ is given by Equation (59). The state-based control signal of Equation (56) is replaced by the hold-based control:

$$u = -\mathbf{k}\mathbf{x}_h + d \tag{65}$$

It is assumed that the controller is associated with a time-delay t_d. As described by Gawthrop et al. (2011, Section 3.3), this delay can be overcome using an *intermittent predictor* which can be written as

$$\mathbf{x}_p(t_i) = \mathbf{E}_{pp}\mathbf{x}(t_i) + \mathbf{E}_{ph}\mathbf{x}_h(t_i) \tag{66}$$

where the $n \times n$ matrices $\mathbf{E}_{pp}$ and $\mathbf{E}_{ph}$ are partitions of the $2n \times 2n$ matrix $\mathbf{E}$:

$$\mathbf{E} = \begin{pmatrix} \mathbf{E}_{pp} & \mathbf{E}_{ph} \\ \mathbf{E}_{hp} & \mathbf{E}_{hh} \end{pmatrix} \tag{67}$$

$$\text{where } \mathbf{E} = e^{\mathbf{A}_{ph}t_d} \tag{68}$$

$$\text{and } \mathbf{A}_{ph} = \begin{pmatrix} \mathbf{A} & -\mathbf{B}\mathbf{k} \\ \mathbf{0}_{n\times n} & \mathbf{A}_c \end{pmatrix} \tag{69}$$

The sample instants t_i are determined by an *event detector* (Gawthrop et al. 2011, Section 3.4). There are two versions of this event detector: an *absolute* version and a *relative* version. The absolute version monitors the system state x and is described by:

$$E_x = \mathbf{x}^T(t)\mathbf{Q}_t\mathbf{x}(t) - q_t \tag{70}$$

where $\mathbf{Q}_t$ is a positive semi-definite matrix and q_t is a scalar. The relative version monitors the difference $\mathbf{e}_{hp}$ between the system state x and the state $\mathbf{x}_h$ of the model of the closed-loop system embedded in the SMH (64) and is described by:

$$E_e = \mathbf{e}_{hp}^T(t)\mathbf{Q}_t\mathbf{e}_{hp}(t) - q_t^2 \tag{71}$$

$$\text{where } \mathbf{e}_{hp}(t) = \mathbf{x}_h(t) - \mathbf{x}(t) \tag{72}$$

In either case, a new sample at time t_i is taken if the error (E_x or E_e as appropriate) exceeds 0 at time t_i and the condition (63) is satisfied.

5 Simulation

This section compares and contrasts the simulated behaviour of four feedback controllers; the numerical para-

Symbol	Equation	Value
L	(1)	260mm
L_p	(3)	329mm
L_z	(13)	92mm
ω_z	(15)	0.316rads^{-1}
k_θ	(21)	3.57
ρ	(22)	0.280
r_g	(25)	134mm
ω_θ	(27)	10.3rads^{-1}
ξ_θ	(28)	0.04
k_p	(31)	0.100
ξ_z	(38)	0.04
Intermittent only		
Δ_{min}	(63)	250ms
t_d	(64)	200ms

Table 1 Simulation Parameters

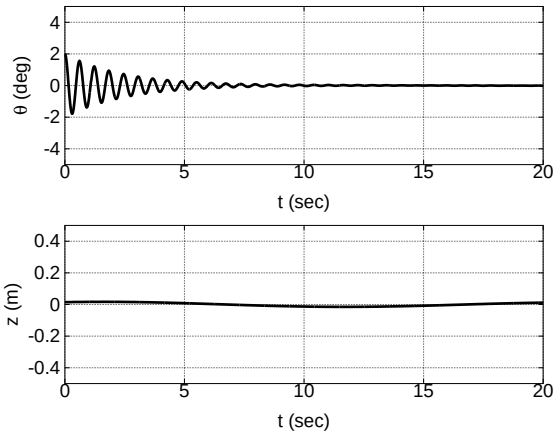

(a) $\sigma_d = 0.001$

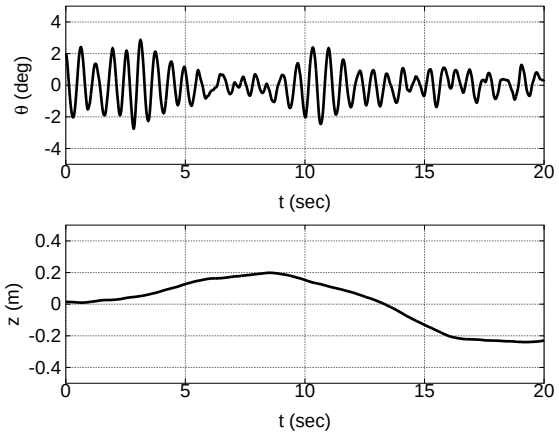

(b) $\sigma_d = 0.3$

Fig. 7 Simulation: continuous control. The initial angle is $\theta = 2^\circ$. (a) The small disturbance gives a purely transient response. (b) The larger disturbance drives both angle θ and translation z to non-zero values. In each case, the angle response is oscillatory.

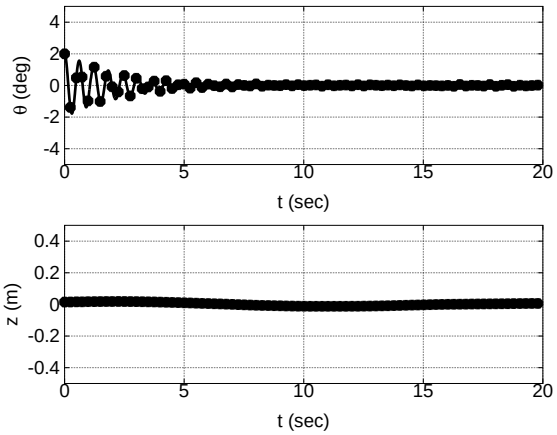

(a) $\sigma_d = 0.001$

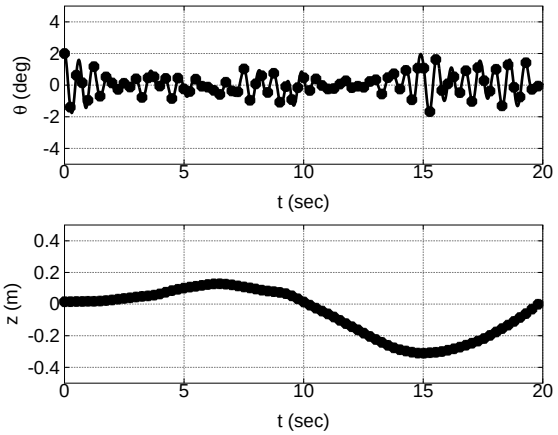

(b) $\sigma_d = 0.03$

Fig. 8 Simulation: intermittent control – zero threshold ($q_t = 0$). The initial angle is $\theta = 2°$, the sample interval is fixed at $\Delta_{min} = 250$ms. (a) The small disturbance gives a purely transient response. (b) The larger disturbance drives both angle θ and translation z to non-zero values. In each case, the angle response is oscillatory.

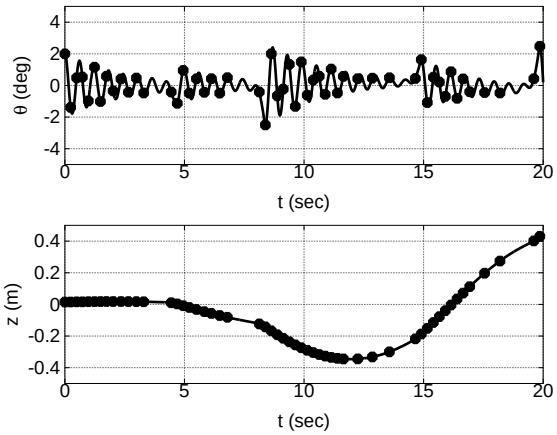

(a) $\sigma_d = 0.001$

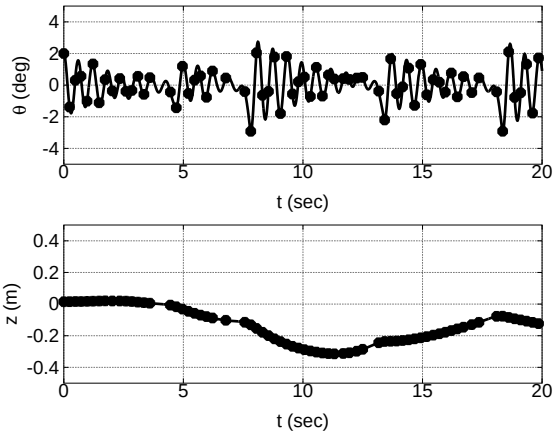

(b) $\sigma_d = 0.01$

Fig. 9 Simulation: intermittent control – absolute threshold $q_t = 0.5°$. The initial angle is $\theta = 2°$. The event-driven control gives similar behaviour for both values of σ_d.

meters appear in Table 1. In each case the input disturbance d is the random multisine signal[3]:

$$d(t) = \sigma_d \sqrt{\frac{2}{N_d}} \sum_{i=1}^{N_d} \sin \omega_i t + \phi_i \tag{73}$$

where $N_d = 1000$, $\omega_i = 0.02\pi i$ and the ith phase angle ϕ_i is a random number drawn from a uniform distribution between 0 and 2π. This signal has a band-limited power spectrum characterised by frequency components equally spaced on the frequency axis at frequencies $0.01, 0.02, \ldots, 10$Hz. It is periodic with period $1/0.01 = 100$sec and the standard deviation is σ_d.

The initial stick angle is 2°. The four feedback controllers are:

1. The continuous-time cascade controller of Section 3 with the state-space representation of Section 3.3 shown in Figure 5 – see Figure 7.
2. The intermittent control of Section 4 shown in Figure 6 with zero threshold ($q_t = 0$) which implies a fixed sample interval of Δ_{min} – see Figure 8.
3. The intermittent control of Section 4 with an *absolute* threshold (Equation (70)) of $q_t = 0.5°$– see Figure 9. This gives a variable sample interval.
4. The intermittent control of Section 4 with a *relative* threshold (Equation (71)) of $q_t = 0.5°$– see Figure 10. This also gives a variable sample interval.

[3] As discussed by, for example, Kasdin (1995), there are a number of approaches to the simulation of random processes. As discussed by, for example Dobrowiecki and Schoukens (2001) and Pintelon and Schoukens (2001), the random multisine is a well-established method for simulating band-limited random processes with clearly defined properties. The random multisine has been used previously in the intermittent control context (Gollee et al. 2012).

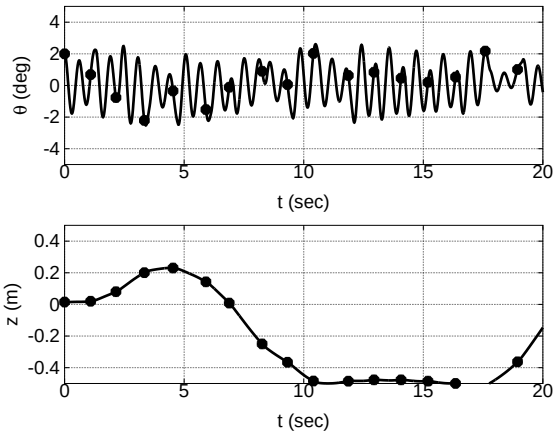

(a) $\sigma_d = 0.001$

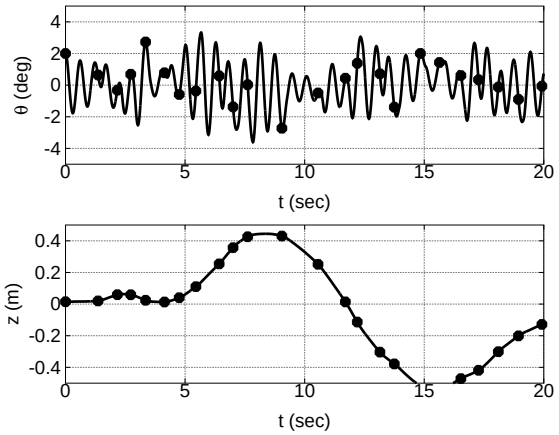

(b) $\sigma_d = 0.01$

Fig. 10 Simulation: intermittent control – relative threshold $q_t = 0.5^\circ$. The initial angle is $\theta = 2^\circ$. The event-driven control gives similar behaviour for both values of σ_d. The behaviour in (a) appears similar to that of a human subject given in Figure 12.

In cases 3&4 the threshold weighting matrix was chosen to weight the state x_2 of Equation (40) corresponding to θ:

$$\mathbf{Q}_t = \begin{bmatrix} 0 & 0 & 0 & 0 \\ 0 & 1 & 0 & 0 \\ 0 & 0 & 0 & 0 \\ 0 & 0 & 0 & 0 \end{bmatrix} \tag{74}$$

The simulation results are shown in Figures 7–10. In Figures 8–10, the sample instants are indicated by •. In the first two cases, the smaller value of σ_d gives an essentially deterministic response from the initial condition whereas the larger value of σ_d gives more random variation in θ and z not unlike the real data. The third and fourth cases have a different behaviour insofar as the system response does not go to zero when σ_d is small. The fourth case gives a random variation in θ and z which is visually not unlike the real data.

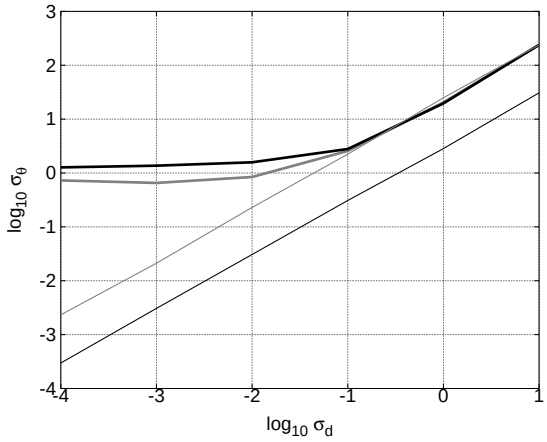

Fig. 11 Variability. The simulated stick angle standard deviation σ_θ is plotted against input noise standard deviation σ_d when using four different controllers (the same noise sequence, suitably scaled, is used in each simulation). The plots in order from the bottom correspond: to continuous control, intermittent control with zero threshold ($q_t = 0$), intermittent control with absolute threshold $q_t = 0.5^\circ$ and intermittent control with relative threshold $q_t = 0.5^\circ$.

Figure 11 examines this behaviour in more detail based on simulations of each controller for a range of σ_d and a simulation length of 100s. The simulated stick angle standard deviation σ_θ is plotted against input noise standard deviation σ_d when using four different controllers (with the same noise sequence – suitably scaled – used in each simulation). The plots in order from the bottom correspond: to continuous control, intermittent control with zero threshold ($q_t = 0$), intermittent control with absolute threshold $q_t = 0.5^\circ$ and intermittent control with relative threshold $q_t = 0.5^\circ$. The first two cases correspond to linear control systems and so, as predicted by theory, σ_θ is proportional to σ_d for continuous control and for zero-threshold intermittent control. In contrast, σ_θ is independent of σ_d for small (relative to q_t) values of σ_d for the two cases of intermittent control with non-zero threshold.

As discussed in Section 4, zero-threshold intermittent control corresponds to a fixed sample interval of Δ_{min} whereas non-zero-threshold intermittent control corresponds to event-driven control leading to a variable sample interval. The variability of event-driven control can be intuitively explained as follows. Because the system is unstable, even a small disturbance is amplified during the intermittent interval when the control is open-loop and thus the event-driven intermittent control has relatively large variance at small disturbance levels. However, for large σ_d, the threshold is overwhelmed by the input noise and thus the two cases of event-driven intermittent control (non-zero threshold) behave as if the threshold were zero.

The simulations of Figures 7–10 can be understood in terms of Figure 11. The continuous-time control of

Figure 7 has small variability for $\sigma_d = 0.001$ but at $\sigma_d = 0.3$ the angle θ has about the same standard deviation as the event-driven controllers at $\sigma_d = 0.001$. Similarly, the intermittent controller with zero threshold of Figure 8 has small variability for $\sigma_d = 0.001$ but at $\sigma_d = 0.03$ the angle θ has about the same standard deviation as the event-driven controllers at $\sigma_d = 0.001$. In contrast, the two event-driven controllers of Figures 9 and 10 have about the same variability at $\sigma_d = 0.001$ and $\sigma_d = 0.01$.

6 Experimental data

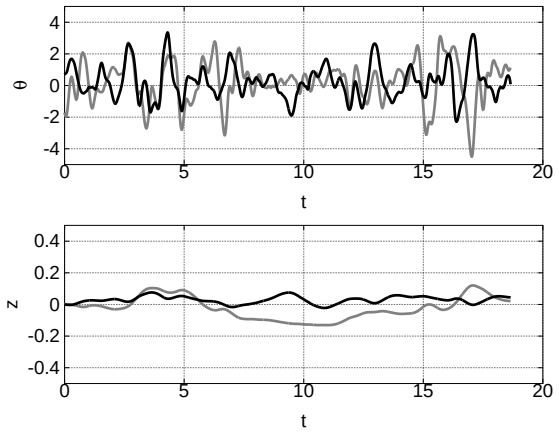

(a) Good subject

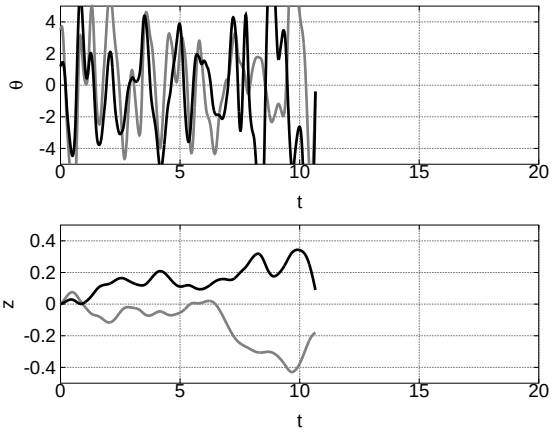

(b) Poor subject

Fig. 12 Real data. The mediolateral motion is shown in black and the anteroposterior data in grey. The "poor" subject drops the stick after about 10s. In both cases, the angular (θ) motion is fast and oscillatory whereas the translational (z) motion is relatively slow.

As described in detail by Lee et al. (2012), fourteen right-handed young adults (6 female, 8 male: aged 18–35 years) performed the task of balancing a stick on the pad of the middle finger of the right hand while standing upright, without moving the feet, for 20 seconds. The stick was a telescopic television antenna (length: 0.52 m, mass: 0.0338 kg, moment of inertia: 0.0029 kg m2, distance from base to centre of mass: 0.26 m). A semi-cone shaped base (diameter: 8 mm), originally the tip of the antenna, was in full contact with the finger pad, preventing slippage between the finger and the base of the stick while balancing. The participants practised for 6 weeks (5 minutes per day, totalling 3.5 hours) and were given a further 10 minutes of practice immediately before data collection. Twenty trials were performed. The experimental procedures were approved by the Human Research Ethics Committee of the University of Sydney and informed written consent was obtained.

In order to track the three-dimensional (3-D) movement of the stick, reflective markers (25 mm diameter Styrofoam spheres [0.56 g] covered with retro-reflective tape) were attached to the stick, one at its tip and the other around the stick 9 cm above its base. The position where the tip of the finger contacted the base of the stick was derived mathematically from the location of the two markers on the stick. Ten cameras (Eagle Cameras, Motion Analysis Corporation, Santa Rosa, CA, USA) were used to track the 3-D movements at 100 Hz. The laboratory coordinate system was defined as ML (medio-lateral), AP (antero-posterior) and V (vertical) axes, paralleling the orientation of the participants at the start of the task.

The subjects were divided into two groups on the basis of those who balanced the pole for more than 15 seconds in more than 15 trials out of 20 (the "good" group) and those who balanced it for less time than this (the "poor" group). Figure 12 shows two typical sets of balancing data in both the mediolateral (ML) and anteroposterior (AP) planes[4]. z is estimated by assuming Equation (25) and using Equations (13) and (8). Figure 12(a) shows the behaviour of a typical "good" subject; although the angle has a strong periodic component, it is kept within about 3° and the horizontal motion is controlled to within about 0.2m. In contrast, Figure 12(b) shows the behaviour of a typical "poor" subject; the stick is dropped after about 10s and both the angle and horizontal motion are larger than that of the "good" subject.

In Figure 12(a) and (b) it can be seen that θ changes more rapidly than z. This reflects the difference between rotational and translational movements of the stick. The movement of the stick approximates to pure translation when the finger (hence the stick base) and stick tip move equal distances in the same direction. In practice, quasi-pure translation can only occur when θ is small, the corresponding gravitational torque on the stick is small and the movements of the finger and stick tip are slow. As the finger moves faster (in response to increased θ), the torque applied to the stick exceeds the gravi-

[4] In this context, mediolateral corresponds to left-right motion and anteroposterior to forward-backwards motion.

tational torque and the stick undergoes rotational motion opposite in direction to that of the finger movement. Hence, at low frequencies the relation between finger position and stick tip position is dominated by translational movement, while at high frequencies the relation between finger position and stick angle is dominated by rotational movement. This was confirmed by cross-correlational and spectrographic analyses of the relation between finger position and stick tip position and between finger position and stick angle. The finger and stick tip positions were highly coupled, in phase (0°), with coherence square values close to unity at frequencies below 0.75 Hz, above which frequency the coherence dropped progressively towards zero by 3 Hz. In contrast, the finger position and stick angle were poorly coupled at low frequencies (coherence < 0.5) but by 0.75 Hz and above, the finger movements were highly coupled (coherence 0.9), out of phase (180°), to stick angle. Thus, the changes in z are slow compared to the changes in θ.

7 Parameter Estimation

This section shows how standard parameter estimation methods (described in Section 7.1) can be used to extract key parameters from experimental data.

This paper suggests that human stick balancing control can be modelled by the intermittent controller of Section 4 which uses the continuous cascade controller of Section 3, in the state-space form of Section 3.3, as the underlying design method. The dynamic response of a closed-loop system containing an intermittent controller can be deduced when the intermittent interval Δ_i (61) is constant (Gawthrop 2009); there is, as yet, no clear result for the more general case. However, in a special case, it has been shown by Gawthrop et al. (2011) that intermittent control *masquerades* as the underlying continuous-time design. Guided by this result, and in the absence of a clear theoretical result, the following assumption is made:

Assumption 1 *The signals arising from the closed-loop system of the intermittent control of Figure 6 can be approximated by those arising for the underlying continuous time design of Figure 5.*

As discussed in Section 3, the damping terms ξ_θ and ξ_z must be non-zero for practical reasons. However, to simplify the subsequent data analysis a further assumption is made:

Assumption 2

$$\xi_\theta = \xi_z = 0$$

The inner-loop of the cascade control of Figure 2 is driven by the outer loop signal θ_0. As discussed in Section 6, it is assumed that the outer loop is slow compared to the inner-loop. This leads to a further assumption:

Assumption 3

$$\theta_0 = 0$$

Using Assumptions 1–3, the continuous-time controller of Section 3.1 implies a closed-loop system where the stick angle θ depends on two signals: the disturbance d and the outer-loop setpoint θ_0. From Equations (23) and (24), and using Assumption 3, θ is related to d by a second-order transfer function:

$$\theta = \frac{\rho}{L_z s^2 + g} d \tag{75}$$

Similarly, using Equations (34) and (35) and setting $z_0 = 0$ and $k_v = 0$, z is also related to d by a second-order transfer function:

$$z = \frac{\rho}{s^2 + k_p} d \tag{76}$$

The parameter estimation method used here is described in Section 7.1 and the validity of Equations (75) and (76) is tested using simulation in Section 7.2. The approach is applied to the real data (described in Section 6) in Section 7.3.

7.1 The state-variable filter method

Parameter estimation in the context of continuous-time systems is a well established topic (Young 1981; Johansson 1994; Unbehauen and Rao 1990; Garnier et al. 2003; Rao and Unbehauen 2006; Garnier and Wang 2008). One approach is based on the *state-variable filter* suggested by Young (1965). Rather than present the general method, this section gives a specific implementation for the systems discussed in this paper.

Define the second-order polynomial $c_\theta(s)$ as

$$c_\theta(s) = s^2 + c_1 s + c_2 \tag{77}$$

Then equation (75) can be rewritten as:

$$\frac{L_z s^2 + g}{c_\theta(s)} \theta = \frac{\rho}{c_\theta(s)} d \tag{78}$$

Defining:

$$\theta_f = \frac{1}{c_\theta(s)} \theta \tag{79}$$

$$\theta''_f = \frac{s^2}{c_\theta(s)} \theta \tag{80}$$

$$\text{and } d_f = \frac{\rho}{g c_\theta(s)} d \tag{81}$$

Equation (75) can be rewritten as:

$$\theta_f = \lambda \theta''_f + d_f \tag{82}$$

$$\text{where } \lambda = -\frac{L_z}{g} \tag{83}$$

The filtered signals θ_f and θ''_f are obtained by passing the measured signal θ through appropriate filters. Given a set of N samples θ_{fi} and θ''_{fi} of the filtered signals indexed by i, an estimate $\hat{\lambda}$ of λ can be obtained from the standard least squares method:

$$\hat{\lambda} = \frac{\sum_{i=1}^{N} \theta''_{fi}\theta_{fi}}{\sum_{i=1}^{N} \theta''^2_{fi}} \tag{84}$$

Using equation (83), an estimate $\hat{L}_z$ of L_z is given by Equation (84) and

$$\hat{L}_z = -g\hat{\lambda} \tag{85}$$

In a similar fashion define z_f and z''_f as

$$z_f = \frac{1}{c_z(s)} z \tag{86}$$

$$z''_f = \frac{s^2}{c_z(s)} z \tag{87}$$

$$\text{where } c_z(s) = s^2 + c_{z1}s + c_{z2} \tag{88}$$

Then using Equation (76), a least-squares estimate $\hat{k}_p$ of k_p is given by:

$$\hat{k}_p = \frac{\sum_{i=1}^{N} z''_{fi} z_{fi}}{\sum_{i=1}^{N} z''^2_{fi}} \tag{89}$$

where z_{fi} and z''_{fi} are the ith samples of z_f and z''_i respectively.

In the case of real data, z is not measured. However, it can be approximately deduced from equations (8) and (13) and the estimate $\hat{L}_z$ from Equation (85) as:

$$\hat{z} = \hat{l}_z\theta - \phi \tag{90}$$

$$\text{where } \hat{l}_z = \hat{L}_z + L_p \tag{91}$$

Thus, in the case of real data, z is replaced by $\hat{z}$ in Equations (86) and (87).

7.2 Simulated data

Figure 13 shows the results of the parameter estimation of Section 7.1 based on the simulations of Section 5. The four simulated "subjects" correspond to

1. continuous-control (Figure 7(b)) with disturbance standard deviation $\sigma_d = 0.3$,
2. zero-threshold intermittent control (Figure 8(b)) with disturbance standard deviation $\sigma_d = 0.03$,
3. absolute threshold intermittent control with $q_t = 0.5°$ (Figure 9(a)) and with disturbance standard deviation $\sigma_d = 0.001$ and
4. relative threshold intermittent control with $q_t = 0.5°$ (Figure 10(a)) and with disturbance standard deviation $\sigma_d = 0.001$.

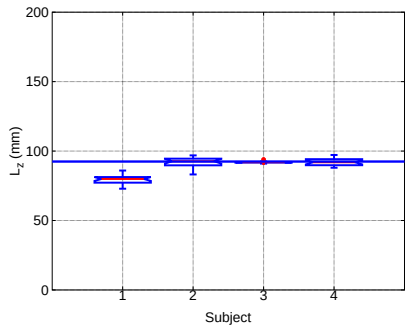

(a) L_z

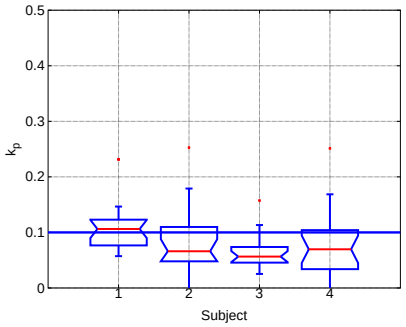

(b) k_p

Fig. 13 Parameter estimation: simulated data. Simulated "subjects" 1–4 are continuous-control (Figure 7(b)), zero-threshold intermittent control (Figure 8(b)), absolute threshold intermittent control (Figure 9(a)) and relative threshold intermittent control (Figure 10(a)) respectively. There are 20 sets of data for each. (a) L_z is estimated from simulated θ, using SVF-based least squares given by Equations (84) and (85). (b) k_p is estimated from simulated z using the estimate of L_z and SVF-based least squares given by Equation (89). The simulated values of L_z and k_p (see Table 1) are marked on (a) and (b) respectively as horizontal lines. Each box plot depicts the median, minimum and maximum values, and the lower and upper quartiles.

With reference to Figure 11, the four values of σ_d correspond to the same order of magnitude angle standard deviation of about $\sigma_\theta = 2°$; this value was chosen to correspond approximately to the behaviour of real subjects.

Each simulation was for 20 sec and 20 sequences were generated for each simulated "subject"; this choice corresponds to the real data. Parameters were identified for each subject and each sequence and the results are shown as box plots in Figure 13.

Although simulated "subjects" 2, 3 and 4 correspond to intermittent, not continuous, control, the estimated parameters correspond closely to those of the underlying continuous-time controller. This phenomenon is related to masquerading (Gawthrop et al. 2011) and has been observed in other contexts (Gollee et al. 2012). The variance of the estimate of k_p is quite large; this is because the data length is quite short compared to the time constants of the horizontal dynamics.

7.3 Real data

As discussed by Lee et al. (2012), data are available in both the mediolateral (ML) and anteroposterior (AP) planes. The data were analysed as discussed above for each of the two groups, and separately in ML and AP directions, and the results displayed in Figure 14 for the "good" group and in Figure 15 for the "poor" group.

The 5 subjects of the "good" group shown in Figure 14, and the 9 subjects of the "poor" group shown in Figure 15, have different estimated values of L_z which are consistent for each subject. Thus angle control using a virtual pivot seems to be a common strategy for all subjects. However, as seen in Figures 14 and 15, the amplitude of the angular motion is larger for the "poor" group than for the "good" group. The 5 subjects of the "good" group shown in Figure 14 again show consistent values for the estimate of k_p in the ML direction, but the value for k_p in the AP direction is more variable as measured by both mean and variance. As discussed by Lee et al. (2012), this may be due to the fact that it is harder for the subject to judge horizontal motion in the AP direction. The 9 subjects of the "poor" group shown in Figure 15 appear to be less consistent in the control of horizontal motion (as evinced by k_p) than the 5 subjects of the "good" group. Moreover, as in the "good" group, control in the AP direction is less consistent than that in the ML direction.

It appears that subjects in both the "good" and "poor" groups adopt the virtual pivot strategy as the values of L_z are consistent for each subject. However, the subjects in the "good" group exhibit smaller angular and translational amplitudes, and more consistent values for the estimate of the translational controller gain k_p, than subjects of the "poor" group.

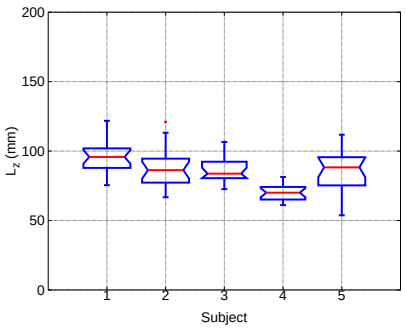

(a) ML: L_z

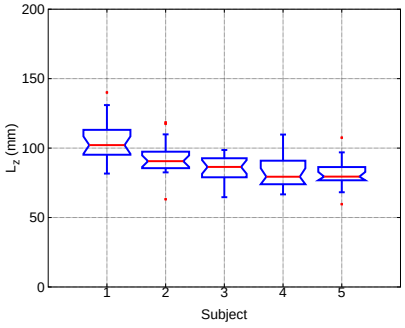

(b) AP: L_z

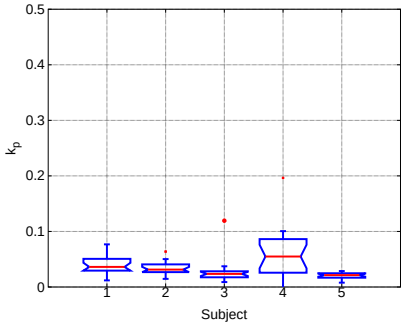

(c) ML: k_p

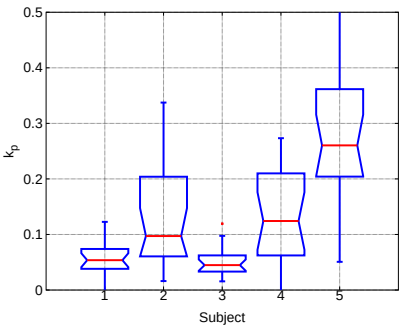

(d) AP: k_p

Fig. 14 Parameter estimation: better subjects. The best (see text) 5 out of 14 subjects are used. (a)&(c) are based on mediolateral (ML) data and (b)&(d) are based on anteroposterior (AP) data. (a)&(b) L_z is estimated from measured θ, using SVF-based least squares given by Equations (84) and (85). (c)&(d) k_p is estimated from measured ϕ using the estimate of L_z and SVF-based least squares given by Equation (89). Each box plot depicts the median, minimum and maximum values, and the lower and upper quartiles ; outliers are plotted as dots.

8 Conclusions

In the context of stick balancing, the virtual pivot of Lee et al. (2012) has been reinterpreted as the key to simultaneously controlling the pendulum angle and the horizontal pendulum position. In particular, the control problem decomposes into the cascade control of two second order systems: control of angle using finger acceleration at an appropriate frequency to create the virtual pivot and control of the horizontal position of the virtual pivot using the pendulum angle controller setpoint.

The continuous cascade controller has been shown to have an intermittent implementation which: accounts for the known intermittency and delay in human control systems, masquerades as a continuous-time controller and explains variability by the event-driven properties of intermittent control rather than by added noise. In practice, the finger/hand/arm system will have dynamics to be included in the design. This could either be achieved explicitly as described by Gawthrop et al. (2011) or im-

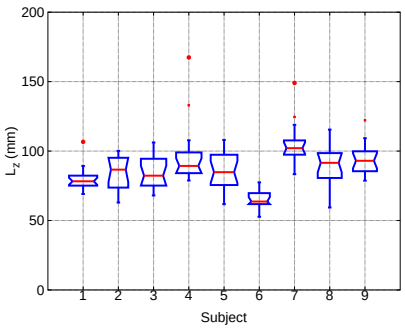

(a) ML: L_z

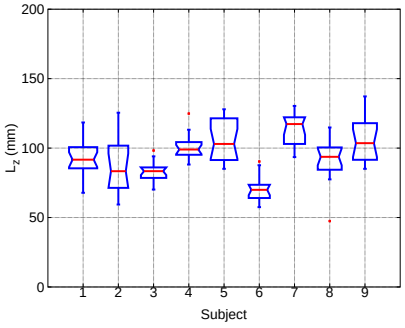

(b) AP: L_z

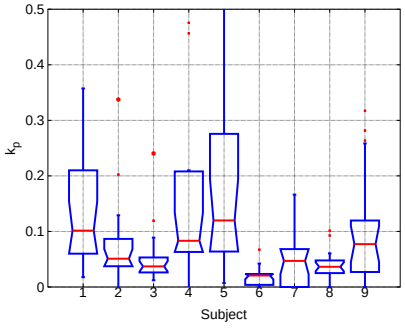

(c) ML: k_p

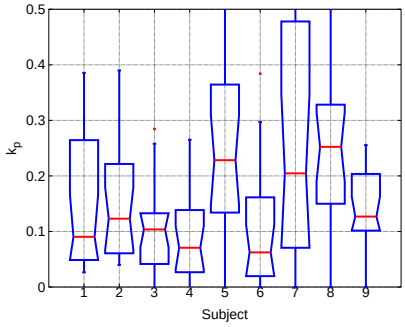

(d) AP: k_p

Fig. 15 Parameter estimation: poorer subjects. The worst (see text) 9 out of 14 subjects are used. (a)&(c) are based on mediolateral (ML) data and (b)&(d) are based on anteroposterior (AP) data. (a)&(b) L_z is estimated from measured θ, using SVF-based least squares given by Equations (84) and (85). (c)&(d) k_p is estimated from measured ϕ using the estimate of L_z and SVF-based least squares given by Equation (89). Not only does each poorer subject have more variability in the estimated parameters than those of the better subjects of Figure 14, but the mean values are more variable between subjects.

plicitly by approximating such dynamics by the pure time delay t_d discussed in Section 4.

Two versions of event-driven intermittent control were presented: *absolute* threshold (70) and *relative* threshold (71). Although the parameter estimation results in Figure 13 are similar in each case, the visual appearance of the simulations shown in Figures 9 & 10 suggest that the latter gives behaviour closer to that of human subjects but both theoretical and experimental research is needed to clarify this point.

The threshold matrix $\mathbf{Q}_t$ of Equations (70) and (71) was chosen in Equation (74) to include only the angle θ. It would be interesting to examine the effect of including other terms such as angular velocity $\dot{\theta}$, translation z and translational velocity $\dot{z}$.

Standard control engineering parameter estimation methods based on the state-variable filter and least-squares are evaluated using simulated data and shown to yield the parameters of the underlying continuous-time controller in the presence of intermittency and delay.

The method is applied to estimate controller parameters from human data. The estimate of L_z (corresponding to the virtual pivot location $\mathbf{V}$) is of low variability for each subject and of similar value between subjects in both ML and AP motion. The estimate of k_p (corresponding to the virtual pivot translation z) is more variable for each subject; this variability is greater for AP motion and is greater for subjects categorised as poor in terms of their ability to stabilise the stick for 20s.

It is known that the standard least-squares approach may be subject to bias due to the properties of d. This suggests two lines of future research: to examine the properties of d corresponding to event-driven intermittent control and to examine more sophisticated parameter identification approaches such as maximum-likelihood (Ljung 1999) and instrumental variables (Young 2011).

The difference between expert and non-expert subjects is manifest in the variability of the k_p estimates. This suggests one way of tracking the progress of learning in human subjects.

The data analysis procedure used here does not distinguish between continuous and intermittent control but rather relies on the masquerading property of intermittent control (Gawthrop et al. 2011). However, it is known that experiments can be devised to explicitly show intermittency (Loram et al. 2012; van de Kamp et al. 2013). It would be interesting to design experiments in the context of stick balancing that could distinguish continuous from intermittent control.

Figure 11, which illustrates how intermittency can explain variability, may provide the basis for experiments that could distinguish event-driven control from continuous-time or fixed sample-interval intermittent control.

Acknowledgements

The work reported here is related to the linked EPSRC Grants EP/F068514/1, EP/F069022/1 and EP/F06974X/1 "Intermittent control of man and machine". Peter Gawthrop was supported by the NICTA Victoria Research Laboratory at the University of Melbourne and is now a Professorial Fellow within the Melbourne School of Engineering; he would also like to acknowledge the many discussions about intermittent control with Ian Loram, Martin Lakie, Henrik Gollee and Liuping Wang.

The authors would like to thank the reviewers for their helpful comments on the draft manuscript.

References

Yoshiyuki Asai, Yuichi Tasaka, Kunihiko Nomura, Taishin Nomura, Maura Casadio, and Pietro Morasso. A model of postural control in quiet standing: Robust compensation of delay-induced instability using intermittent activation of feedback control. *PLoS ONE*, 4(7):e6169, 07 2009.

K.J. Astrom and K. Furuta. Swinging up a pendulum by energy control. *Automatica*, 36(2):287–295, 2000.

Alessandra Bottaro, Maura Casadio, Pietro G. Morasso, and Vittorio Sanguineti. Body sway during quiet standing: Is it the residual chattering of an intermittent stabilization process? *Human Movement Science*, 24(4):588–615, 2005.

Alessandra Bottaro, Youko Yasutake, Taishin Nomura, Maura Casadio, and Pietro Morasso. Bounded stability of the quiet standing posture: An intermittent control model. *Human Movement Science*, 27(3):473–495, 2008.

Olfa Boubaker. The inverted pendulum: A fundamental benchmark in control theory and robotics. In *Education and e-Learning Innovations (ICEELI), 2012 International Conference on*, pages 1–6, July 2012.

Juan L. Cabrera and John G. Milton. On-off intermittency in a human balancing task. *Phys. Rev. Lett.*, 89(15):158702, 2002.

Kenneth J Craik. Theory of human operators in control systems: Part 1, the operator as an engineering system. *British Journal of Psychology*, 38:56–61, 1947.

T.P. Dobrowiecki and Johan Schoukens. Practical choices in the FRF measurement in presence of nonlinear distortions. *Instrumentation and Measurement, IEEE Transactions on*, 50(1):2–7, 2001.

Isabelle Fantoni and Rogelio Lozano. Stabilization of the Furuta pendulum around its homoclinic orbit. *Int. J. Control*, 75(6):390–398, April 2002.

R Fitzpatrick and D I McCloskey. Proprioceptive, visual and vestibular thresholds for the perception of sway during standing in humans. *The Journal of Physiology*, 478(Pt 1):173–186, 1994.

H. Garnier, M. Mensler, and A. Richard. Continuous-time model identification from sampled data: Implementation issues and performance evaluation. *International Journal of Control*, 76(13):1337–1357, 2003.

Hugues Garnier and Liuping Wang, editors. *Identification of continuous-time models from sampled data*. Advances in Industrial Control. Springer, London, 2008.

Peter Gawthrop, Ian Loram, and Martin Lakie. Predictive feedback in human simulated pendulum balancing. *Biological Cybernetics*, 101(2):131–146, 2009a.

Peter Gawthrop, Ian Loram, Martin Lakie, and Henrik Gollee. Intermittent control: A computational theory of human control. *Biological Cybernetics*, 104(1-2):31–51, 2011.

Peter J Gawthrop. Frequency domain analysis of intermittent control. *Proceedings of the Institution of Mechanical Engineers Pt. I: Journal of Systems and Control Engineering*, 223(5):591–603, 2009.

P.J. Gawthrop, M.D. Lakie, and I.D. Loram. Predictive feedback control and Fitts' law. *Biological Cybernetics*, 98(3): 229–238, March 2008.

P.J. Gawthrop, D.J. Wagg, and S.A. Neild. Bond graph based control and substructuring. *Simulation Modelling Practice and Theory*, 17(1):211–227, January 2009b.

H. Gollee, A. Mamma, I. D. Loram, and P. J. Gawthrop. Frequency-domain identification of the human controller. *Biological Cybernetics*, 106:359372, 2012.

G.C. Goodwin, S.F. Graebe, and M.E. Salgado. *Control System Design*. Prentice Hall, New Jersey, 2001.

Tamas Insperger, John Milton, and Gabor Stepan. Acceleration feedback improves balancing against reflex delay. *Journal of The Royal Society Interface*, 10(79), February 2013.

R. Johansson. Identification of continuous-time models. *Signal Processing, IEEE Transactions on*, 42(4):887–897, apr 1994.

Amir Karniel. Open questions in computational motor control. *Journal of Integrative Neuroscience*, 10(3):385–411, 2011.

N.J. Kasdin. Discrete simulation of colored noise and stochastic processes and 1/f alpha; power law noise generation. *Proceedings of the IEEE*, 83(5):802–827, May 1995.

D. Kleinman, S. Baron, and W. Levison. A control theoretic approach to manned-vehicle systems analysis. *Automatic Control, IEEE Transactions on*, 16(6):824–832, Dec 1971.

D. L. Kleinman, S. Baron, and W. H. Levison. An optimal control model of human response part I: Theory and validation. *Automatica*, 6:357–369, May 1970.

Piotr Kowalczyk, Paul Glendinning, Martin Brown, Gustavo Medrano-Cerda, Houman Dallali, and Jonathan Shapiro. Modelling human balance using switched systems with linear feedback control. *Journal of The Royal Society Interface*, 2011.

H. Kwakernaak and R. Sivan. *Linear Optimal Control Systems*. Wiley, New York, 1972.

K-Y. Lee, N. ODwyer, M. Halaki, and R. Smith. A new paradigm for human stick balancing: a suspended not an inverted pendulum. *Experimental Brain Research*, pages 1–20, 2012.

Lennart Ljung. *System Identification: Theory for the User*. Information and Systems Science. Prentice-Hall, 2nd edition, 1999.

Ian D. Loram and Martin Lakie. Human balancing of an inverted pendulum: position control by small, ballistic-like, throw and catch movements. *Journal of Physiology*, 540(3):1111–1124, 2002.

Ian D. Loram, Martin Lakie, and Peter J. Gawthrop. Visual control of stable and unstable loads: what is the feedback delay and extent of linear time-invariant control? *J Physiol*, 587(6):1343–1365, 2009.

Ian D. Loram, Cornelis van de Kamp, Henrik Gollee, and Peter J. Gawthrop. Identification of intermittent control in man and machine. *Journal of The Royal Society Interface*, 9(74):2070–2084, 2012.

David Marr. *Vision. A Computational Investigation into the Human Representation and Processing of Visual Information*. W.H. Freeman, San Francisco, 1982. ISBN 0716712849.

Biren Mehta and Stefan Schaal. Forward models in visuomotor control. *Journal of Neurophysiology*, 88(2):942–953, 2002.

J.G. Milton, J.L. Cabrera, and T. Ohira. Unstable dynamical systems: Delays, noise and control. *EPL (Europhysics Letters)*, 83(4):48001, 2008.

John G Milton. The delayed and noisy nervous system: implications for neural control. *Journal of Neural Engineering*, 8(6):065005, 2011.

John G. Milton, Toru Ohira, Juan Luis Cabrera, Ryan M. Fraiser, Janelle B. Gyorffy, Ferrin K. Ruiz, Meredith A. Strauss, Elizabeth C. Balch, Pedro J. Marin, and Jeffrey L. Alexander. Balancing with vibration: A prelude for drift and act balance control. *PLoS ONE*, 4(10):e7427, 10 2009.

Fernando Navas and Lawrence Stark. Sampling or Intermittency in Hand Control System Dynamics. *Biophys. J.*, 8 (2):252–302, 1968.

P.D. Neilson, M.D. Neilson, and N.J. O'Dwyer. Internal models and intermittency: A theoretical account of human tracking behaviour. *Biological Cybernetics*, 58:101–112, 1988.

Romi Nijhawan and Si Wu. Compensating time delays with neural predictions: are predictions sensory or motor? *Philosophical Transactions of the Royal Society A: Mathematical, Physical and Engineering Sciences*, 367(1891): 1063–1078, 2009.

Yalchin Oytam, Peter D. Neilson, and Nicholas J. O'Dwyer. Degrees of freedom and motor planning in purposive movement. *Human Movement Science*, 24(5-6):710– 730, 2005.

Rik Pintelon and Johan Schoukens. *System Identification. A frequency domain approach*. IEEE press, 2001.

G.P. Rao and H. Unbehauen. Identification of continuous-time systems. *Control Theory and Applications*, 153(2): 185–220, March 2006.

Eckehard Scholl, Gerald Hiller, Philipp Hovel, and Markus A Dahlem. Time-delayed feedback in neurosystems. *Philosophical Transactions of the Royal Society A: Mathematical, Physical and Engineering Sciences*, 367(1891):1079–1096, 2009.

R. Shadmehr and S.P. Wise. *Computational Neurobiology of Reaching and Pointing: A Foundation for Motor Learning*. MIT Press, Cambridge, MA, 2005.

Marilyn C. Smith. Theories of the psychological refractory period. *Psychological Bulletin*, 67(3):202–213, March 1967.

Gabor Stepan. Delay effects in the human sensory system during balancing. *Philosophical Transactions of the Royal Society A: Mathematical, Physical and Engineering Sciences*, 367(1891):1195–1212, 2009.

Yasuyuki Suzuki, Taishin Nomura, Maura Casadio, and Pietro Morasso. Intermittent control with ankle, hip, and mixed strategies during quiet standing: A theoretical proposal based on a double inverted pendulum model. *Journal of Theoretical Biology*, 310(0):55 –79, 2012.

C W. Telford. The refractory phase of voluntary and associative responses. *Journal of Experimental Psychology*, 14 (1):1–36, February 1931.

Emanuel Todorov and Michael I. Jordan. Optimal feedback control as a theory of motor coordination. *Nature Neuroscience*, 5(11):1226–1235, November 2002.

H. Unbehauen and G.P. Rao. Continuous-time approaches to system identificationa survey. *Automatica*, 26(1):23–35, 1990.

Cornelis van de Kamp, Peter J. Gawthrop, Henrik Gollee, and Ian D. Loram. Refractoriness in sustained visuomanual control: Is the refractory duration intrinsic or does it depend on external system properties? *PLoS Comput Biol*, 9(1):e1002843, 01 2013.

M.A. Vince. The intermittency of control movements and the psychological refractory period. *British Journal of Psychology*, 38:149–157, 1948.

Dmitry Volkinshtein and Ron Meir. Delayed feedback control requires an internal forward model. *Biological Cybernetics*, 105:41–53, 2011. ISSN 0340-1200.

P. C. Young. The determination of the parameters of a dynamic process. *Radio and Electronic Engineer*, 29:345–361, 1965.

Peter Young. Parameter estimation for continuous-time models: A survey. *Automatica*, 17(1):23–39, 1981.

Peter C. Young. *Recursive Estimation and Time-Series Analysis: An Introduction for the Student and Practitioner*. Springer, Berlin, Heidelberg, 2011. ISBN 978-3-642-21980-1.